Role of boundaries in micromagnetic calculations of magnonic spectra of arrays of magnetic nanoelements

O. Dmytriiev and V. V. Kruglyak*
School of Physics, University of Exeter, Exeter, EX4 4QL, United Kingdom

M. Franchin and H. Fangohr
Engineering and the Environment, University of Southampton, SO17 1BJ, United Kingdom

L. Giovannini and F. Montoncello
Dipartimento di Fisica, Università di Ferrara, Via G. Saragat 1, 44122 Ferrara, Italy
(Received 20 December 2012; revised manuscript received 17 April 2013; published 20 May 2013)

We have used micromagnetic simulations performed with open and periodic boundary conditions to study the influence of the presence of array boundaries on the spectra and spatial profiles of collective spin-wave excitations in arrays of magnetic nanoelements. The spectra and spatial profiles of collective spin waves excited in isolated arrays of nanoelements and those forming a part of quasi-infinite arrays are qualitatively different even if the same excitation field is used in the simulations. In particular, the use of periodic boundary conditions suppresses the excitation of nonuniform collective modes by uniform excitation fields. However, the use of nonuniform excitation fields in combination with periodic boundary conditions is shown to enable investigation of the structure of magnonic dispersion curves for quasi-infinite arrays (magnonic crystals) in different directions in the reciprocal space and for different magnonic bands. The results obtained in the latter case show a perfect agreement with those obtained with the dynamical matrix method for infinite arrays of nanoelements of the same geometry and magnetic properties.

DOI: 10.1103/PhysRevB.87.174422 PACS number(s): 75.78.Cd, 75.40.Mg, 75.30.Ds, 75.75.−c

I. INTRODUCTION

The recent advances in nanofabrication techniques have stimulated intense interest in studying static and dynamic properties of various artificial periodic magnetic structures—magnonic crystals.[1–6] In particular, investigations of propagating and standing spin waves in such structures are in the focus of one of the youngest areas of magnetism—magnonics.[7,8] From the point of view of technological applications, the study of spin waves in periodic magnetic structures has attracted a great deal of attention for two main reasons. First, an in-depth understanding of collective precessional dynamics is necessary to master the magnetic switching of magnetic memory cells (i.e., magnetic recording) at increasingly high data rates.[9] Second, spin waves in nanoscale magnetic structures promise alternative ways to transmit and process information, potentially not involving electrical currents.[7,10] Being a magnetic counterpart of photonic crystals, magnonic crystals are expected to give a full control of the dispersion of spin waves. At the same time, the phenomenon of hysteresis[11] and the associated ability of magnetic nanostructures to form multiple micromagnetic states offer additional opportunities and challenges for research inquiry into fundamental physics of magnetism. In particular, the spectrum and dispersion of spin waves in arrays of magnetic elements and other magnonic crystals can be controlled and programmed externally, e.g., by the strength and direction of the applied (bias) magnetic field or even by the history of their variation.[12,13]

Two-dimensional (2D) arrays of magnetic nano- and microelements[14–18] and antidots[19–22] of various shapes form the most actively studied class of magnonic crystals. Experimentally, spin waves in such arrays are studied using ferromagnetic resonance (FMR),[23] time-resolved scanning Kerr microscopy (TRSKM),[12] Brillouin light-scattering (BLS) spectroscopy,[21,24] and other techniques.[7] The experimental results obtained using these techniques are interpreted using either reciprocal space semianalytical approaches, such as the plane-wave method[25,26] and the modified version of the dynamical matrix method (DMM),[27,28] or time and real space micromagnetic simulations.[12,24,29–31] In the latter case, the limited available computational power does not normally allow one to run simulations for realistic samples, often extending to tens and even hundreds of micrometers in both in-plane directions. Hence, the simulations are performed for smaller systems, albeit using different approaches for arrays of magnetic elements and antidots. In the case of antidots, periodic boundary conditions (PBCs) are applied to relatively small arrays, often just to one unit cell.[32,33] Quite surprisingly, precessional dynamics in arrays of magnetic elements are usually interpreted using simulations performed for finite and then quite small (normally just 3×3) arrays of such elements without the use of PBCs.[34–36] There are only a few works in which PBCs are employed in micromagnetic simulations for arrays of magnetic elements.[37]

PBCs are realized differently in different micromagnetic packages. The underlying aim is, however, always the same: to suppress the effect of the finite size of the sample, i.e., to modify the internal field in a finite sample so that it could be treated as a part of a larger one. Full micromagnetic simulations are carried out within this representative finite sample, which is typically called a primary cell (or unit cell). To calculate the internal field in the primary cell with account of the contribution from the larger sample (in which the primary cell is only a part), a sufficiently large (and sometimes infinite) number of image cells (or virtual cells) is introduced. Every

image cell is obtained by translating the primary cell by a translation vector (which is often a linear combination of integer numbers of orthogonal basis translation vectors) in space, and the magnetization dynamics in every image cell is assumed by definition to be the same as that in the primary cell. Hence, the image cells do not contribute additional degrees of freedom to the computational complexity of the problem. Indeed, the magnetization dynamics in the primary cell are simulated as if it were an ordinary (i.e., finite) micromagnetic system, with the only difference that the magnetic dipolar field is computed taking into account contributions from all image cells. In the case of the magnetic material in the primary and image cells being in direct contact, one would also need to consider the exchange interaction across the interfaces, leading to coupling of the magnetization at one end of the primary cell to that at its opposite end. However, this is not necessary for the arrays of magnetic elements considered in this work.

The conventional implementation of PBCs takes into account an infinite number of image cells. In micromagnetic simulations, one-dimensional (1D)[38] and 2D[39] PBCs with an infinite number of image cells are available, for example, for the object oriented micromagnetic framework (OOMMF). A somewhat different approach has been proposed under the name of macrogeometry[40] in which only a finite number of image cells are used. These can be placed at arbitrary positions in space, although the primary and image cells should not overlap. Thereby, as opposed to the infinite PBCs, the macrogeometry allows one to simulate a large yet finite sample by choosing a finite number of image cells and distributing them spatially so as to approximate its shape and dimensions. Hence, the choice of the name macrogeometry: the union of the primary cell and the virtual cells describes the geometry of the macroscopic sample that one wishes to simulate. The demagnetizing field experienced by the primary cell depends on the shape of the entire sample. For example, a spherical primary cell embedded within a 1D row of virtual cells will experience a strongly anisotropic demagnetizing field (with the anisotropy axis being parallel to the axis of the rod), whereas the same primary cell embedded in an appropriate spherical arrangement of virtual cells will experience an isotropic demagnetizing field (if the magnetization in the primary cell is uniform; see also Sec. I in Ref. 40). Furthermore, the demagnetizing field experienced by the primary cell in the first example of a rodlike macrogeometry will depend on the number of virtual image cells, which corresponds to the length of the rod. The macrogeometry approach allows us to fully take into account these geometrical characteristics of the sample that we want to simulate. In contrast, the conventional PBCs with an infinite number of image cells can only describe two geometries: that of an infinitely long rod (with 1D PBCs) and that of an infinite plane (with 2D PBCs).

We state for completeness that, in addition to systems exhibiting (quasi) periodicity in 1D and 2D systems, the macrogeometry can also be used for three-dimensional (3D) systems, which is impossible for the infinite PBCs.[40] We also note that the conventional PBCs with infinitely many image cells are a special case of the macrogeometry approach. Indeed, the macrogeometry approach becomes the same method as the conventional PBCs (with an infinite number of image cells), if the image cells are placed on a regular 1D or 2D grid of a lattice

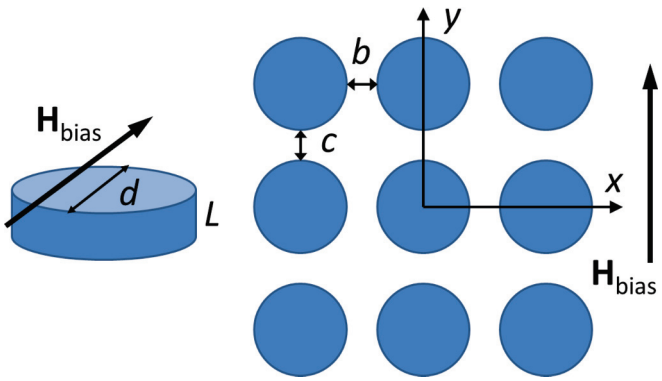

FIG. 1. (Color online) The geometry used in the simulations is shown. The thickness and diameter of the disks are $L = 2.5$ nm and $d = 50$ nm, respectively. The in-plane edge-to-edge separation is $c = b = 2.5$ nm. The bias magnetic field $H_{\text{bias}} = 2.5$ kOe is applied in the plane of the array along the y axis.

points and the number of image cells is increased to infinity. The contributions to the demagnetizing field in the primary cell decay as the distance between image cells and the primary cell increases. So, in practice, it is sufficient to use a finite number of image cells to obtain a numerically identical demagnetizing field in the primary cell. This is indeed the approach used to compute the demagnetizing tensor in the implementation of the PBCs in OOMMF: contributions from image cells are added until they are so small that the required numeric accuracy is achieved. In the example of a single line of image cells centred around the primary cell, the macrogeometry approach with ten image cells closely stacked to either side of the primary cell yielded a demagnetizing field comparable to that calculated using the infinite PBCs (see Fig. 1 and example 1 in Ref. 40).

In this work, we use the finite element package NMAG,[41] which provides an implementation of the macrogeometry to systematically study the influence of the finite size (and therefore the existence of boundaries) of arrays of magnetic nanoelements on the spectrum and profiles of their precessional modes. In the remainder of the manuscript, the term PBCs refers to the use of the macrogeometry approach with a finite number of image cells, which is specified for each of the studies.

Unlike isolated magnetic elements, for which the influence of the inhomogeneity of the internal magnetic field at their edges on the magnonic spectrum has been thoroughly investigated,[42–45] the influence of the lateral boundaries of finite arrays of magnetic nanoelements on their spectrum has not been investigated in much detail. In the present paper, we compare the spectra of collective standing spin waves in isolated arrays of permalloy disk-shaped elements with those in the same arrays surrounded by different numbers of virtual image cell arrays. The results are discussed in terms of the micromagnetic model choice (open versus PBCs) for interpretation of experimental results produced by different techniques. In addition, we demonstrate how one can investigate the structure of magnonic dispersion curves of quasi-infinite arrays. We show how the position of the edges of magnonic bands and band gaps along different directions in the reciprocal space can be determined from micromagnetic simulations with PBCs (or macrogeometry approach) and

spatially nonuniform excitation fields applied to small arrays of just a few nanoelements. The results obtained with this method are shown to be in perfect agreement with those obtained within the DMM. So far, PBCs have been used in micromagnetic simulations only with spatially uniform excitation fields, thereby limiting results to uniform collective excitations. Hence, the proposed approach increases the range of problems of magnonics that may be successfully solved using micromagnetic simulations.[46]

II. NUMERICAL MODEL

We consider arrays of magnetic disks with thickness $L = 2.5$ nm and diameter $d = 50$ nm. The edge-to-edge separation between the elements in the arrays is $c = b = 2.5$ nm (Fig. 1). We performed simulations with different numbers of disks in the primary cell (i.e., primary array): from a single disk to a 5×5 array. In each case, two simulations were performed: one with open boundary conditions (isolated array) and one with the use of the 2D macrogeometry approach applied along two orthogonal directions in the plane of the array. In the latter case, the number of virtual copies was chosen so that the dimensions of large (virtual) arrays with the primary array in the middle were always similar (about 1.31×1.31 μm^2), while the total number of elements was greater than or equal to 25×25. So, for the 5×5, 4×4, 3×3, and 2×2 arrays of elements and for the single element, we took 2, 3, 4, 6, and 12 virtual images on each side of the primary cell, respectively. The same mesh size of 1.25 nm was used in each case. In the simulations, we assumed the saturation magnetization of $M_S = 860$ G, and the exchange stiffness constant of $A = 1.3$ μerg/cm. We assumed a magnetic damping constant of $\alpha = 0.0001$ in order to reduce the width of peaks in the spectrum. The constant bias magnetic field of $H_{bias} = 2.5$ kOe was applied in the plane of the disks along y (vertical) direction.

We used the standard procedure to find the spectrum of spin-wave excitations. First, we calculated the static magnetization configuration of the system. The obtained magnetic ground state was used as the initial magnetization configuration in the dynamical simulations in which the sample was excited by an in-plane magnetic pulse with amplitude of $h = 18$ Oe and duration of 10 ps applied perpendicularly to the bias magnetic field. We considered both spatially uniform and nonuniform excitation fields applied to different parts of the arrays. We recorded the magnetization dynamics for 32.8 ns and saved the spatially resolved magnetization every 10 ps. The time- and space-resolved data were used to calculate the spectra and associated spatial mode profiles with help of SEMARGL software.[47]

III. STATIC INTERNAL DEMAGNETIZING FIELD AS A FUNCTION OF THE NUMBER OF VIRTUAL COPIES

The spatial profile of the static demagnetizing field is one of the main factors determining the mode spectrum of magnetic nanoelements.[34,37,42] So, in this section, we study the variation of the profile of the demagnetizing field in individual elements as a function of the number of elements in the array. In the static simulations, it is sufficient to consider a system with a single disk in the primary cell. Figure 2 shows the spatial profiles of the projection of the static demagnetizing field on the direction of the bias field for an isolated disk and a disk in the center of 3×3, 9×9, and 21×21 arrays (i.e., for cases of 1, 4, and 10 virtual copies on each side of the disk, respectively). The spatial dimensions of the 3×3, 9×9, and 21×21 virtual arrays are $155 \times 155 \times 2.5$ nm^3 (the aspect ratio is 0.016), $470 \times 470 \times 2.5$ nm^3 (0.0053), and $1100 \times 1100 \times 2.5$ nm^3 (0.0023), respectively.

Figure 2 reveals deep demagnetized "wells" at the ends of an isolated disk along the direction of the bias field. The depth of the wells significantly decreases as the number of elements in the virtual array increases. Small demagnetized wells are also formed near the ends along the direction perpendicular to the bias field. The depth of the wells increases as the number of elements in the virtual array increases. However, the strength and profile of the demagnetizing field in the central element show almost no variation as the size of the virtual array is increased from 9×9 to 21×21 elements. This shows that the numbers of virtual copies of the primary arrays assumed in the present study are large enough to extrapolate our conclusions to models in which the primary arrays would be located in the middle of infinite arrays. We therefore refer to them as "quasi-infinite" in the rest of the paper.

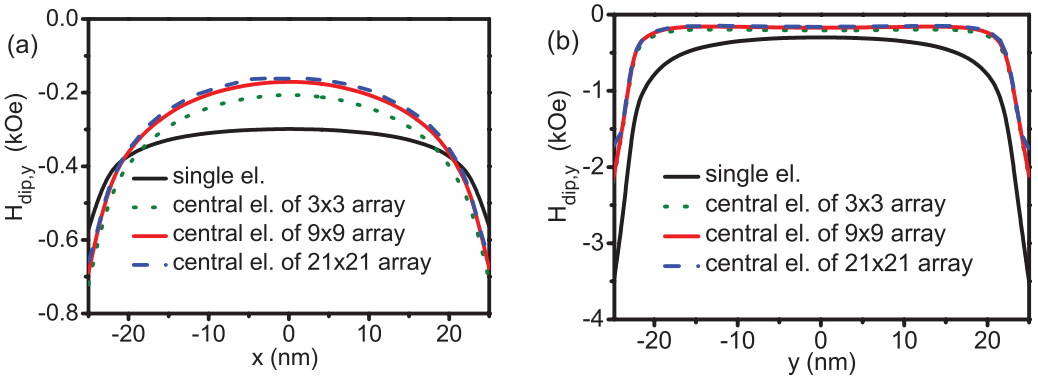

FIG. 2. (Color online) The spatial profiles of the projection of the static demagnetizing field on the direction of the bias field (i.e., y axis) is shown for an isolated disk and the same disk in the center of the 3×3, 9×9, and 21×21 arrays. Panels (a) and (b) correspond to the profiles along the x and y axes, respectively.

IV. SPECTRA AND SPATIAL PROFILES OF PRECESSIONAL MODES IN FINITE AND EFFECTIVELY INFINITE ARRAYS

In this section, we compare the spectra and associated mode profiles of isolated disk arrays (open boundary conditions) and the same arrays forming a part of larger (quasi-infinite) arrays (PBCs). In both cases, we have used spatially uniform magnetic fields to excite magnetization dynamics. Figure 3 shows spectra of spin-wave excitations of 1×1, 2×2, 3×3, 4×4, and 5×5 arrays of disks with and without the use of PBCs in micromagnetic simulations. The spectra calculated from data simulated with the use of PBCs resemble closely the spectrum of an isolated element, with the blueshift of the resonant frequencies being the only significant difference. In contrast, the spectra of isolated arrays contain many additional peaks in comparison to the isolated element. Similar to the previous work,[12,14] the additional peaks are attributable to collective modes of the arrays of finite size. The excitation of the modes by the spatially uniform pulsed fields is enabled by distortion of the periodicity of the internal field at the array boundaries. At the same time, the modes are not visible in the simulations with PBCs since the latter suppress the boundary effects associated with the finite size of the arrays and thereby also suppress the ability of the nonuniform collective modes to couple to the uniform pulsed fields.

Figure 4 compares the amplitude and phase of spin-wave modes in an isolated disk and semi-infinite arrays simulated with either a single disk or a 3×3 array of those in the primary cell. As before, the pulsed field is uniform and applied in the plane of the disks perpendicular to the bias magnetic field. The spectrum and mode profiles of isolated magnetic elements in the quasiuniform ground state of various, e.g., rectangular,[37] elliptical,[48,49] stadiumlike,[50] and round,[36,51–53] shapes were extensively studied by experimental, numerical, and analytical means. For rectangular elements, it is possible to use the mode classification scheme derived in Ref. 54 from the one for spin waves in continuous magnetic films. In particular, one can distinguish Damon-Eshbach-like modes (nDE; n is the number of nodal lines parallel to the static magnetization),

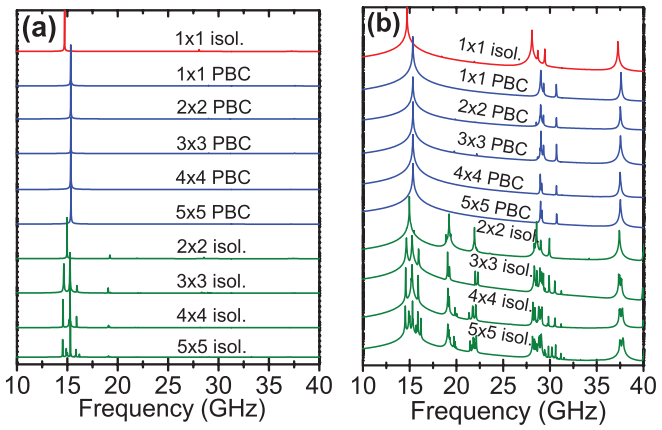

FIG. 3. (Color online) The spectra of spin-wave excitations in isolated arrays and semi-infinite arrays are shown in linear (a) and logarithmic (b) scales. The different curves are arbitrarily offset along the y axis for visual clarity.

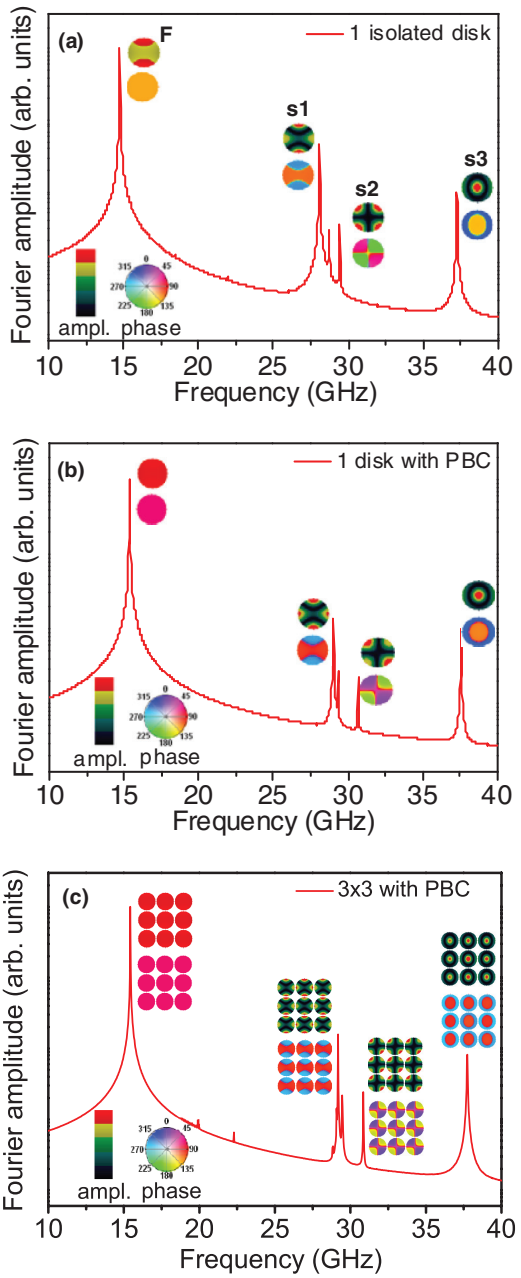

FIG. 4. (Color online) The amplitude (top) and phase (bottom) of spin-wave excitations are shown for an isolated disk (a) and for semi-infinite arrays with a single disk (b) and a 3×3 array of those (c) in the primary cell. The bias magnetic field is applied vertically in the plane of the figure.

backward-volume-like modes (mBA; m is the number of nodal lines perpendicular to the static magnetization), the fundamental (F) mode (or quasiuniform mode, characterized by the absence of nodes within an element), and edge modes (EM; localized at the edges of an element). Finally, the EM can also be subdivided into DE-like and BA-like modes, depending on the presence of corresponding nodal lines in the region of its localization. One can see from Fig. 4 that this classification is not fully applicable to disk-shaped elements in which the nodal lines have a complicated structure because of the round shape. However, we will be able to use this classification to

label collective excitations in the square arrays due to their square symmetry.

The dominant peak in the spectrum of an isolated disk corresponds to a mode the amplitude of which near the ends is greater than that in the central region of the disk. However, the mode profile does not really split into two separate edge regions, as it would be expected for an EM.[34] Hence, it is more appropriate to classify the mode as the F (quasiuniform) rather than EM. This is consistent with the fact that the frequency of the mode is close to that of the uniform FMR of a tangentially magnetized ferromagnetic film. The other modes of the isolated disk have nodal lines within the disk plane and are labeled here as s1, s2, and s3. The modes have much greater frequencies in comparison with the F mode. This indicates that the dominant contribution to their frequencies originates from the exchange interaction, leading to the positive dispersion of the modes.

The spatially uniform pulsed field used in the simulations cannot excite antisymmetric modes of the disk. However, such modes could be excited in simulations with nonuniform pulsed fields.[55] For example, by applying the pulsed field only to the disk's upper (or lower) part, we could excite a mode with the amplitude profile similar to that of s1 but with the opposite ends oscillating out of phase—antisymmetric s1.[48,50] However, such modes are beyond this study.

Figures 4(b) and 4(c) show that the modes retain their character in the simulations for semi-infinite arrays with both one disk and a 3×3 array of those in the primary cell. The only exception is the F mode that gets fully uniform due to the suppression of the demagnetized regions at the disk ends. The resonant frequencies also experience significant blueshift (e.g., 0.56 GHz for the dominant peak) due to the demagnetizing field produced by the virtual images. We note that this behavior is in contrast to that of truly edge localized mode profiles of which were found to be rather soft in Refs. 35 and 50.

As mentioned earlier, the distortion of the periodic internal field in the vicinity of the boundaries of isolated arrays leads to excitation of additional collective modes, which cannot be excited by uniform pulsed fields in the same arrays forming part of semi-infinite arrays. To study this effect, let us consider the spatial profiles of precessional modes of an isolated 3×3 array that are shown on Fig. 5. As a result of a strong magnetodipole interaction, the mode profiles vary somewhat from element to element since the elements experience different fields and have different ground states, depending on their position within the 3×3 array. However, by comparing the spectra (Fig. 3) and mode profiles (Fig. 4) of a single element and a 3×3 array, the origin of the collective modes can still be traced back to modes of a single element.

Let us use the classification scheme described above for a square element to classify the collective modes by their spatial character. We will need to note that the nodal line can fall into the gap between elements. We will add the name of the single-element mode to that of the associated collective

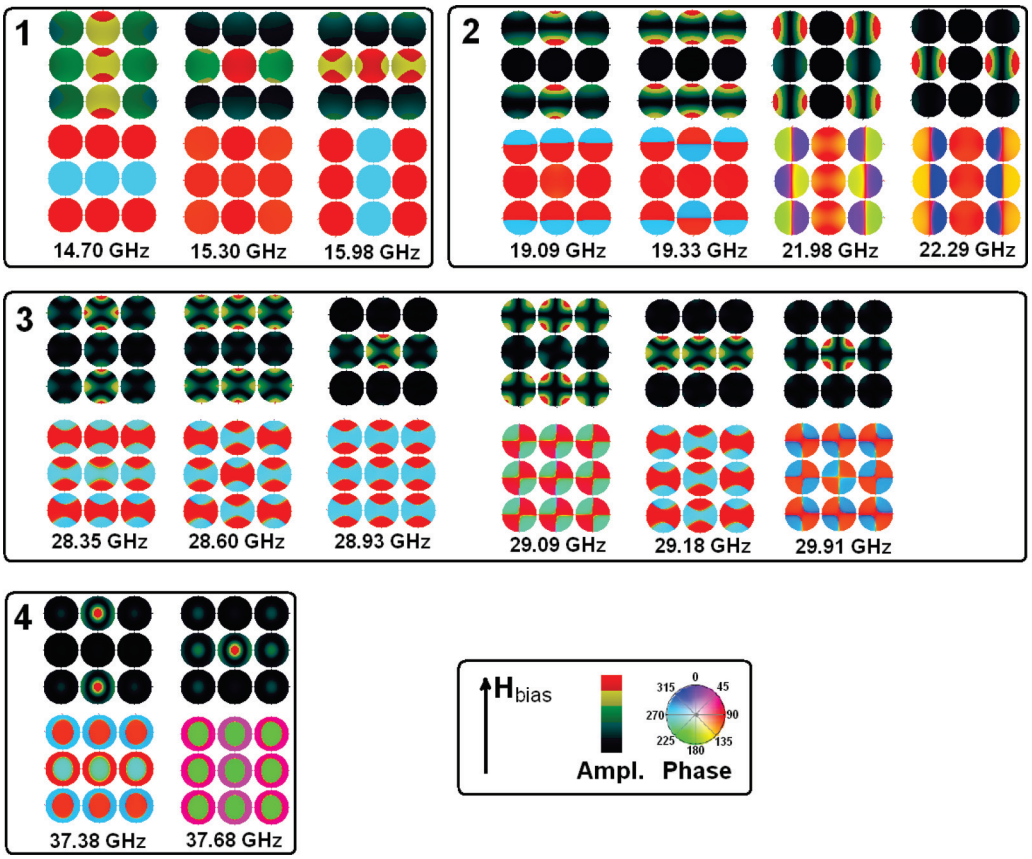

FIG. 5. (Color online) The amplitude (top) and phase (bottom) of spin-wave modes in an isolated 3×3 array of magnetic disks are shown. The modes are grouped in the different panels according to their spatial character compared to modes of a single element. The bias magnetic field is applied vertically in the plane of the figure.

modes. For convenience, we group the collective modes by their origin into the four sets shown in the different panels of Fig. 5. The first set of collective modes originates from the F mode of a single element. It consists of three modes with different values of the k vector: a nonzero k vector along the bias field (F-2BA), a zero k vector (uniform collective mode, i.e., F-U) and a nonzero k vector perpendicular to the direction of the bias field (F-2DE). Due to the anisotropy inherent to the magnetodipole interaction, the frequency shifts of the F-2BA and F-2DE modes relative to the F-U one have opposite signs, as was observed, e.g., in Refs. 12 and 14. However, the frequency shifts are very similar in value, although it is known that the dispersion of DE modes is generally stronger than that of BA modes. This is attributable to an additional decrease of the F-2BA mode frequency resulting from the reduction of the internal magnetic field caused by the demagnetizing field from the magnetic charges at the boundaries of the array as a whole that are perpendicular to the applied magnetic field. Indeed, as opposed to the F-2DE and F-U modes, the F-2BA mode has significant amplitude in the boundary rows of disks that are orthogonal to the direction of the applied magnetic field.

Set 2 consists of the modes localized in the boundary rows and columns of the array. These modes originate from antisymmetric modes of a single element, for which the opposite ends of the disk oscillate out of phase and which therefore has not been observed in the simulations for a single element and a uniform pulsed magnetic field. We call them here "boundary modes," in analogy to edge (end) modes of isolated elements. The two lowest-frequency modes have zero amplitude in the central row and can therefore be classified as localized in the boundary rows. The latter are demagnetized, thereby reducing the frequency of the modes. The two higher-frequency modes have nearly zero amplitude in the central column and can therefore be classified as localized in the boundary columns. The highest frequency mode in the set has nearly zero amplitude in the demagnetized regions of the array. The second boundary mode (counting from left to right) has a DE character, which leads to positive dispersion and an increased frequency relative to the first mode, which has a zero k vector. Similarly, the third mode has an additional (relative to the fourth mode) phase variation in the direction parallel to the applied magnetic field and is therefore of the BA volume character. This leads to a negative dispersion and a reduced frequency relative to that of the fourth mode in the set. At the same time, the increased frequency of the third and fourth modes relative to the first two modes in the set is in due to the amplitude profile in individual elements. Indeed, unlike the first and second modes, the amplitude of the third and fourth modes is localized near the disk ends (edges) that lie along the applied field. This diminishes the effect of the demagnetization by the static magnetic charges formed at the ends (edges) orthogonal to the applied field, whereas the dynamical magnetic charges at the ends that lie along the applied field lead to the positive frequency dispersion.

Set 3 consists of the modes originating from the s1 and s2 modes of a single element: s1-2BA, s1-2BA2DE, s1-U, s2-U, s1-DE, s2-BA modes. Set 4 consists of the modes originating from the s3 mode of a single element. The frequency variation of the different modes within the sets can be interpreted using the same considerations as in the case of sets 1 and 2.

V. MICROMAGNETIC SIMULATIONS WITH PBC AND A SPATIALLY NONUNIFORM EXCITATION FIELD: INVESTIGATION OF THE DISPERSION STRUCTURE OF QUASI-INFINITE ARRAYS

As we have seen, collective modes with nonzero k vectors of arrays of magnetic nanoelements with suppressed boundary effects have a reduced coupling to uniform pulsed fields. So, to excite and then study such modes in micromagnetic simulations with PBCs (in which the internal magnetic field correctly corresponds to infinite arrays), we should use spatially nonuniform excitation fields instead. The smallest and largest possible finite "collective" wavelengths of modes with nonzero k vectors that could be excited in simulations with PBCs are equal to twice the period of the primary array (which corresponds to the k vector exactly at the edge of the Brillouin zone) and to the size of the primary array, respectively. So, by properly choosing the dimensions of the primary array and the spatial profile of the excitation field, one can access collective modes of any wavelength and therefore any k vector within the Brillouin zone of the corresponding quasi-infinite array. We illustrate this approach using the same simple square array of disk-shaped nanoelements. We then compare results of such micromagnetic simulations with the results of the DMM calculations, which have already been successfully used to investigate band diagrams in large arrays of nanoelements.[56]

In the present case of a quasi-infinite array with a simple square lattice, to obtain the frequencies of the collective modes at the bottom (zero k vector) and boundaries of the Brillouin zone from simulations with PBCs, it is sufficient to consider a 2×2 primary cell excited by a spatially nonuniform pulsed field. Figure 6 shows on a logarithmic scale the mode spectra of an isolated 2×2 array with (blue solid lines) and without (red dashed line) application of PBCs. The simulations with PBCs are repeated for different spatial profiles of the pulsed field, as schematically represented above each line: only the black-colored area is subjected to a uniform (in this area)

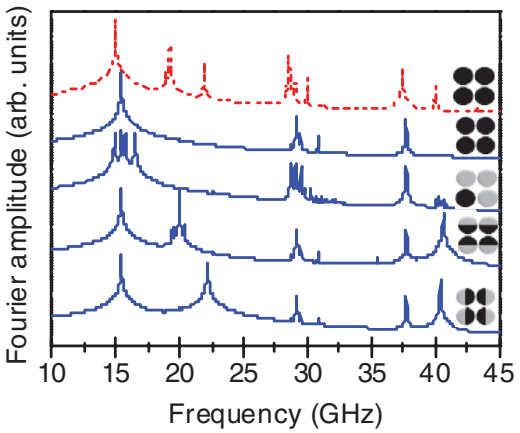

FIG. 6. (Color online) The mode spectra are shown on logarithmic scale for an isolated 2×2 array (red dashed line) and for the same array simulated with application of PBCs (blue solid lines). The spatial configuration of the pulsed magnetic field used in the simulations is schematically shown above each line so that the area of the array subjected to a uniform pulsed field is marked by black color.

pulsed field. One can see that the selective application of a pulsed field to only one disk in the primary array in simulations with PBCs leads to a splitting of the dominant spectral peaks. At the same time, the application of the uniform field to central region along the different orthogonal directions leads to excitation of additional collective modes as compared to the same array excited by a globally uniform pulsed field. Below, we will identify the mode character and collective k vectors by analyzing the spatial profiles of the modes.

Figure 7 shows the mode profiles (top) and phase (bottom) of spin wave corresponding to dominant peaks of the spectra shown in Fig. 6. The spectrum and spatial character of modes in an isolated 2×2 array shown on Fig. 7(a) are qualitatively similar to those described above for an isolated 3×3 array. So, we concentrate on modes with nonzero k vectors in quasi-infinite arrays in the following discussion. In the simulations with the pulsed field applied to only one disk in the primary cell [Fig. 7(b)], the F mode of a single disk splits into the BA, uniform, mixed BA-like, DE-like (mixed BA-DE), and DE modes of the quasi-infinite array. The first, third, and fourth modes (listed in the order of increasing frequency) correspond to spin waves with their k vector exactly at the edges of the Brillouin zone along different directions in the reciprocal space. The second mode corresponds to the k vector at the bottom of the Brillouin zone. The calculated splitting of the F mode of a single element as a result of interaction within the array enables us to analyze the magnonic dispersion along different directions in the reciprocal space. So, we observe the expected negative and positive dispersions for the BA-like and DE-like spin-wave modes, respectively. Furthermore, due to the mentioned fact that the dynamic coupling is stronger in the direction perpendicular to the bias field as compared to that in the parallel direction, we observe that the splitting (and therefore the width of the allowed band) is two times greater for DE-like spin waves than for BA-like ones, i.e., 1.06 GHz against 0.53 GHz. The effect of this anisotropic coupling also manifests itself in that the mixed BA-DE mode shows a positive dispersion. The second set of the modes originates from the splitting of the s1 mode of a single element. The modes correspond to the BA-like, uniform, and DE-like spin waves of the quasi-infinite array. The splitting and therefore the width of the magnonic bands are substantially smaller (0.43 and 0.36 GHz) than in the case of the F mode. The third set consists of just one mode originating from the s2 mode of a single element, and the last peak originates from the s3 one of a single element. In both of the latter cases, the splitting of the modes is below the resolution of the simulations, set by the used value of the damping constant and the duration of each simulation.

To excite in quasi-infinite square array the collective modes with other spatial symmetries within individual elements [e.g., such as those shown in panels (2)–(4) of Fig. 5], we applied the pulsed field to the middle region of the primary array along different orthogonal directions, as shown above the curves on Figs. 7(c) and 7(d). In the case shown in Fig. 7(c), we observe excitation of BA-like collective modes originating

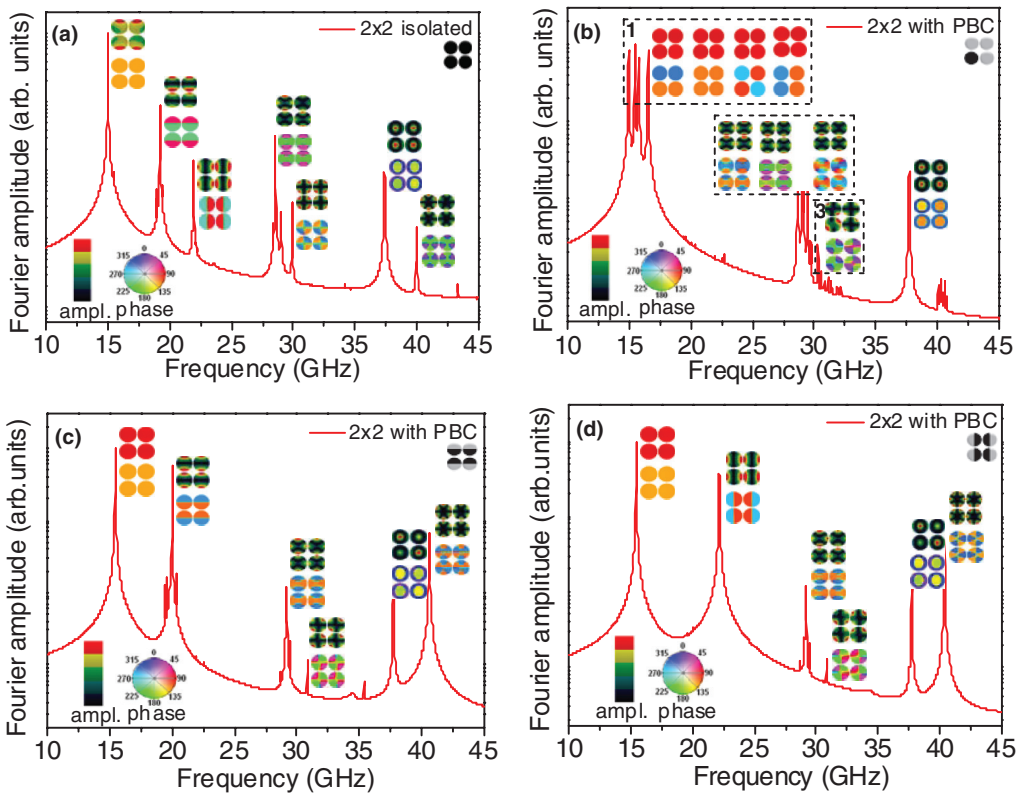

FIG. 7. (Color online) The mode profiles (top) and phase (bottom) of spin-wave modes in (a) an isolated 2×2 array and (b)–(d) quasi-infinite arrays with a 2×2 primary array. The spatial configuration of the pulsed field used in the simulations is schematically shown in the right top corners of each panel, with the area of the array uniformly excited by the pulsed field marked by black color. The bias magnetic field is applied vertically in the plane of the figure.

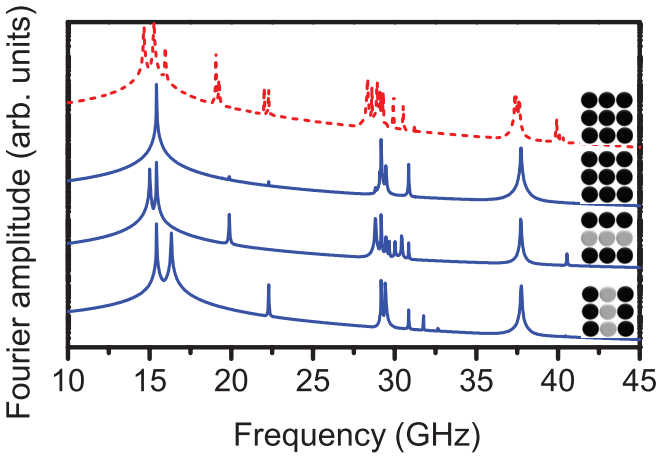

FIG. 8. (Color online) The spectra of spin-wave excitations are shown on the logarithmic scale for an isolated 3×3 array (red dashed line) and the same array as the primary cell in the simulations with PBCs (blue solid lines). The spatial configuration of the pulsed field is schematically shown above each line, with the area of the array to which the uniform pulsed field is applied marked by black color.

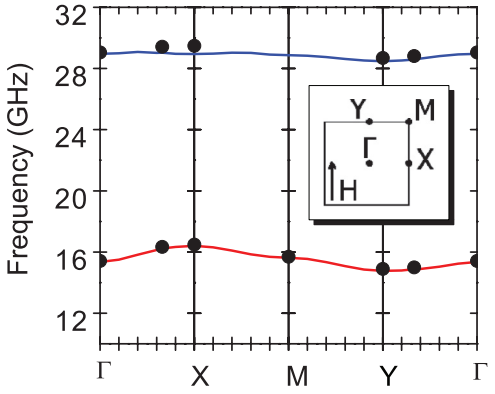

FIG. 10. (Color online) The magnonic band diagram calculated using the DMM is shown for two bands corresponding to mode sets 1 and 2 shown in Fig. 7(b). The frequency of the modes obtained from the micromagnetic simulations are shown by black dots. The inset shows the corresponding Brillouin zone and the direction of the bias magnetic field.

from the antisymmetric mode of a single element (the second dominant peak from the left). In the case shown in Fig. 7(d), we observe excitation of the DE-like collective modes originating from the orthogonally oriented (relative to the applied field) antisymmetric mode of a single element (the second dominant peak from the left). In both cases, the k vectors correspond to the Brillouin zone boundaries.

To calculate frequencies of the collective excitations in semi-infinite arrays with the wavelength greater than two periods of the array (i.e., with the k vector within rather than at the edges of the Brillouin zone), we need to consider primary arrays larger than the 2×2 array discussed so far. We will demonstrate the calculation considering a 3×3 array in the primary cell in micromagnetic simulation with PBCs and a spatially nonuniform pulsed field. So, Fig. 8 shows on a logarithmic scale the spectra of spin-wave excitations in an isolated 3×3 array (red dashed line) and the same array in the primary cell of a semi-infinite array (blue solid lines). Again, the spatial configuration of the pulsed magnetic field is schematically shown above each line. The corresponding mode profiles are shown in Fig. 9. To excite BA-like and DE-like modes, we applied an excitation pulse to the top and bottom rows and to the left and right columns of the primary array, respectively. As expected, we observe splitting of the corresponding modes of a single element into BA-like (with the wavelength of three periods of the semi-infinite array) and uniform modes, in the former case, and into uniform and DE-like modes, in the latter case.

Let us compare the spectra obtained from the results of the micromagnetic simulations with PBCs with the magnonic band diagram calculated for an infinite square array of magnetic nanodisks of the same geometry using the DMM approach. So, Fig. 10 presents two magnonic bands calculated by the DMM that correspond to mode sets 1 and 2 shown in Fig. 7(b). The frequencies of the modes obtained from the micromagnetic simulations are shown in Fig. 10 by black dots. The inset shows the corresponding directions in the reciprocal space within the first Brillouin zone. Table I compares the

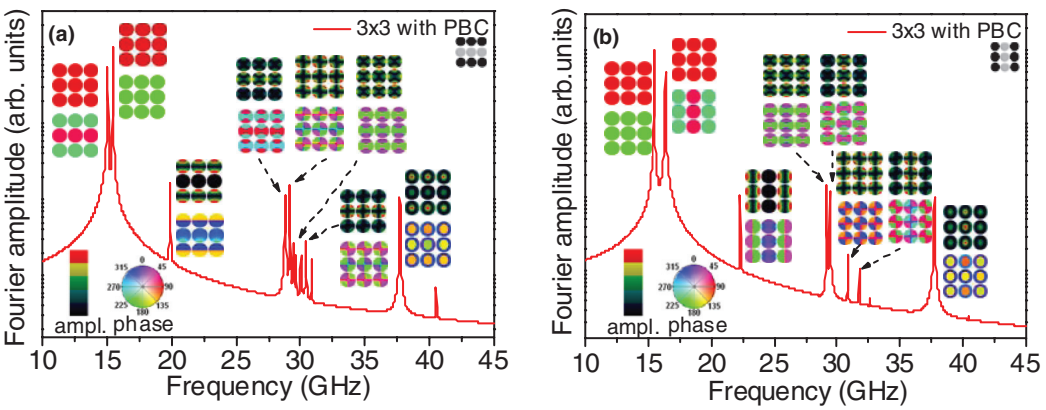

FIG. 9. (Color online) The spatial profiles of the amplitude (top) and phase (bottom) of spin-wave modes in a quasi-infinite array are shown as calculated from simulations with a 3×3 primary array with PBCs. The spatial configuration of the pulsed field is schematically shown above each line, with the area of the array to which the uniform pulsed field is applied marked by black color. The bias magnetic field is applied vertically in the plane of the figure.

TABLE I. The frequencies calculated for the symmetry points within the first Brillouin zone comparing the DMM and micromagnetic simulations (Nmag).

	Γ		X		M		Y	
	DMM	Nmag	DMM	Nmag	DMM	Nmag	DMM	Nmag
First band	15.3 GHz	15.4 GHz	16.4 GHz	16.5 GHz	15.6 GHz	15.7 GHz	14.8 GHz	14.9 GHz
Second band	29.1 GHz	29.1 GHz	28.9 GHz	29.5 GHz	28.9 GHz	–	28.5 GHz	28.7 GHz

frequency values obtained by the two approaches. It is evident that both methods produce nearly perfect agreement, with a less than 0.1-GHz deviation for the first of the bands. For the second band, the DMM and micromagnetic simulations yield the same frequencies at Γ and close frequency values at M and Y, within 0.6- and 0.2-GHz deviation, respectively, corresponding to 2 and 0.07% of the average frequency values, respectively.

VI. DISCUSSION

Let us briefly discuss the obtained results in view of using micromagnetic simulations to analyze data produced by different experimental techniques. The TRSKM technique[12,14,34] acquires data in the time and real-space domains, which is the same as results produced by micromagnetic simulations. In both cases, the time-resolved data are converted into the frequency domain using Fourier analysis. The TRSKM data are therefore most naturally suited for comparison with and interpretation by micromagnetic simulations. The formation of collective magnonic modes in arrays of interacting magnetic elements often manifests itself via splitting of the resonance modes of an isolated magnetic element serving as the building block of the array.[12,14] The simulations presented in this paper demonstrate that the splitting becomes observable due to the presence of boundaries of the finite-sized arrays modeled with open boundary conditions. This is consistent with the finite size of the arrays measured in Refs. 12 and 14. Furthermore, our simulations suggest that the splitting could not be observed if the micromagnetic simulations in Refs. 12 and 14 were performed with PBCs. However, it is also clear that it would be quite difficult if at all possible to achieve quantitative agreement between the TRSKM data and simulations in terms of the splitting and absolute values of the collective mode frequencies, unless the size of the array in simulations matched that in the experiment, suggesting the origin of the quantitative discrepancies observed in Ref. 57. The arrays studied in Refs. 12 and 14 measured 4×4 μm^2, while the constituent elements were down to 40×80 nm^2 in size. Unfortunately, the computational power required for modeling of such samples is still beyond that currently available to micromagnetic simulations.

In contrast to the TRSKM technique, the BLS measurements are usually performed on much larger arrays. Moreover, the sensitivity of the BLS measurements to thermally excited spin waves means that the formation of collective modes can be observed in arrays of any size and structure, provided that the interaction between the constituent elements is strong enough. Under such circumstances, the proposed combined use of the PBCs and the nonuniform excitation would be particularly appropriate, for example, in the case of the results similar to those reported in Refs. 35 and 36. An experimental verification of the method is however beyond the scope of this report. Overall, the DMM approach combined with the Bloch theorem[27] appears most appropriate and computationally efficient if the aim is to reproduce the dispersion of collective spin waves in infinite arrays. Yet, in the case of finite-sized arrays, the DMM faces the same limitations in terms of computing power as those outlined in the preceding paragraph for micromagnetic simulations performed in the time domain.

VII. CONCLUSIONS

In summary, we have studied the influence of the presence of lateral boundaries on the spectrum and profiles of collective spin-wave excitations in finite-sized arrays of magnetic elements. We have compared the spectra and spatial profiles of spin-wave modes in isolated arrays of nanoelements and in the same arrays as building blocks of quasi-infinite arrays formed within a macrogeometry approach in micromagnetic simulations. We have shown that, in contrast to the isolated arrays, the collective excitations with nonzero k vectors do not couple to spatially uniform excitation fields in arrays with boundary effects suppressed by the macrogeometry so that only uniform collective spin-wave modes (with the collective k vector equal to zero) can be excited. However, the collective excitations with finite collective k vectors could be excited in simulations with a spatially nonuniform excitation field. Finally, we have demonstrated that the structure of magnonic dispersion curves for quasi-infinite arrays along different directions in the reciprocal space and in different allowed bands could be investigated using simulations for small arrays of just a few nanoelements with application of PBCs. The PBCs have been widely used in micromagnetic simulations for arrays of antidots and in rare occasions for arrays of nanoelements. However, the latter simulations have only been performed with spatially uniform excitation fields, limiting the results to uniform collective spin waves. Our results obtained using time domain micromagnetic simulations are in perfect agreement with those obtained using the DMM approach for infinite arrays of nanoelements.

ACKNOWLEDGMENTS

The research leading to these results has received funding from the ECs 7th Framework Programme (FP7/2007-2013) under Grant No. 233552 (DYNAMAG) and from EPSRC of the UK under Project No. EP/E055087/1.

*Corresponding author: V.V.Kruglyak@exeter.ac.uk

[1] S. A. Nikitov, P. Tailhades, and C. S. Tsai, J. Magn. Magn. Mater. **236**, 320 (2001).

[2] M. Krawczyk, J.-C. Lévy, D. Mercier, and H. Puszkarski, Phys. Lett. A **282**, 186 (2001).

[3] S. Mamica, M. Krawczyk, M. L. Sokolovskyy, and J. Romero-Vivas, Phys. Rev. B **86**, 144402 (2012).

[4] B. Lenk, N. Abeling, J. Panke, and M. Münzenberg, J. Appl. Phys. **112**, 083921 (2012).

[5] Y. Filimonov, E. Pavlov, S. Vystostkii, and S. Nikitov, Appl. Phys. Lett. **101**, 242408 (2012).

[6] M. Mruczkiewicz, M. Krawczyk, V. K. Sakharov, Y. V. Khivintsev, Y. A. Filimonov, and S. A. Nikitov, J. Appl. Phys. **113**, 093908 (2013).

[7] V. V. Kruglyak, S. O. Demokritov, and D. Grundler, J. Phys. D **43**, 264001 (2010), and references therein.

[8] B. Lenk, H. Ulrichs, F. Garbs, and M. Münzenberg, Phys. Rep. **507**, 107 (2011), and references therein.

[9] J. W. Lau and J. M. Shaw, J. Phys. D **44**, 303001 (2011).

[10] J.-H. Kim, K.-S. Lee, H. Jung, D.-S. Han, and S.-K. Kim, Appl. Phys. Lett. **101**, 092403 (2012).

[11] G. Bertotti, *Hysteresis in Magnetism* (Academic Press, San Diego, 1998).

[12] P. S. Keatley, V. V. Kruglyak, A. Neudert, E. A. Galaktionov, R. J. Hicken, J. R. Childress, and J. A. Katine, Phys. Rev. B **78**, 214412 (2008).

[13] J. Topp, S. Mendach, D. Heitmann, M. Kostylev, and D. Grundler, Phys. Rev. B **84**, 214413 (2011).

[14] V. V. Kruglyak, P. S. Keatley, A. Neudert, R. J. Hicken, J. R. Childress, and J. A. Katine, Phys. Rev. Lett. **104**, 027201 (2010).

[15] R. Zivieri, F. Montoncello, L. Giovannini, F. Nizzoli, S. Tacchi, M. Madami, G. Gubbiotti, G. Carlotti, and A. O. Adeyeye, Phys. Rev. B **83**, 054431 (2011).

[16] S. Mamica, M. Krawczyk, and J. W. Klos, Adv. Condens. Matter Phys. **2012**, 161387 (2012).

[17] J. W. Klos, M. L. Sokolovskyy, S. Mamica, and M. Krawczyk, J. Appl. Phys. **111**, 123910 (2012).

[18] B. Rana, D. Kumar, S. Barman, S. Pal, R. Mandal, Y. Fukuma, Y. Otani, S. Sugimoto, and A. Barman, J. Appl. Phys. **111**, 07D503 (2012).

[19] M. Kostylev, G. Gubbiotti, G. Carlotti, G. Socino, S. Tacchi, C. Wang, N. Singh, A. O. Adeyeye, and R. L. Stamps, J. Appl. Phys. **103**, 07C507 (2008).

[20] S. Neusser, G. Duerr, H. G. Bauer, S. Tacchi, M. Madami, G. Woltersdorf, G. Gubbiotti, C. H. Back, and D. Grundler, Phys. Rev. Lett. **105**, 067208 (2010).

[21] S. Tacchi, M. Madami, G. Gubbiotti, G. Carlotti, A. O. Adeyeye, S. Neusser, B. Botters, and D. Grundler, IEEE Trans. Magn. **46**, 172 (2010).

[22] R. Mandal, S. Saha, D. Kumar, S. Barman, S. Pal, K. Das, A. K. Raychaudhuri, Y. Fukuma, Y. Otani, and A. Barman, ACS Nano **6**, 3397 (2012).

[23] O. N. Martyanov, V. F. Yudanov, R. N. Lee, S. A. Nepijko, H. J. Elmers, R. Hertel, C. M. Schneider, and G. Schönhense, Phys. Rev. B **75**, 174429 (2007).

[24] H. T. Nembach, J. M. Shaw, T. J. Silva, W. L. Johnson, S. A. Kim, R. D. McMichael, and P. Kabos, Phys. Rev. B **83**, 094427 (2011).

[25] M. Krawczyk and H. Puszkarski, Phys. Rev. B **77**, 054437 (2008).

[26] H. Yang, G. Yun, and Y. Cao, J. Appl. Phys. **112**, 103911 (2012).

[27] L. Giovannini, F. Montoncello, and F. Nizzoli, Phys. Rev. B **75**, 024416 (2007).

[28] R. Zivieri, F. Montoncello, L. Giovannini, F. Nizzoli, S. Tacchi, M. Madami, G. Gubbiotti, G. Carlotti, and A. O. Adeyeye, IEEE Trans. Magn. **47**, 1563 (2011).

[29] F. S. Ma, H. S. Lim, Z. K. Wang, S. N. Piramanayagam, S. C. Ng, and M. H. Kuok, IEEE Trans. Magn. **47**, 2689 (2011).

[30] R. Rückriem, P. Krone, T. Schrefl, and M. Albrecht, Appl. Phys. Lett. **100**, 242402 (2012).

[31] L. Lopez-Diaz, D. Aurelio, L. Torres, E. Martinez, M. A. Hernandez-Lopez, J. Gomez, O. Alejos, M. Carpentieri, G. Finocchio, and G. Consolo, J. Phys. D **45**, 323001 (2012).

[32] S. Tacchi, M. Madami, G. Gubbiotti, G. Carlotti, A. O. Adeyeye, S. Neusser, B. Botters, and D. Grundler, IEEE Trans. Magn. **46**, 1440 (2010).

[33] S. Neusser, B. Botters, and D. Grundler, Phys. Rev. B **78**, 054406 (2008).

[34] V. V. Kruglyak, A. Barman, R. J. Hicken, J. R. Childress, and J. A. Katine, Phys. Rev. B **71**, 220409 (2005).

[35] S. Tacchi, M. Madami, G. Gubbiotti, G. Carlotti, H. Tanigawa, T. Ono, and M. P. Kostylev, Phys. Rev. B **82**, 024401 (2010).

[36] G. Gubbiotti, M. Madami, S. Tacchi, G. Carlotti, and T. Okuno, J. Appl. Phys. **99**, 08C701 (2006).

[37] C. Bayer, J. Jorzick, B. Hillebrands, S. O. Demokritov, R. Kouba, R. Bozinoski, A. N. Slavin, K. Y. Guslienko, D. V. Berkov, N. L. Gorn, and M. P. Kostylev, Phys. Rev. B **72**, 064427 (2005).

[38] K. M. Lebecki, M. J. Donahue, and M. W. Gutowski, J. Phys. D **41**, 175005 (2008).

[39] W. Wang, C. Mu, B. Zhang, Q. Liu, and J. Wanf, Comput. Mater. Sci. **49**, 84 (2010).

[40] H. Fangohr, G. Bordignon, M. Franchin, A. Knittel, P. A. J. de Groot, and T. Fischbacher, J. Appl. Phys. **105**, 07D529 (2009).

[41] T. Fischbacher, M. Franchin, G. Bordignon, and H. Fangohr, IEEE Trans. Magn. **43**, 2896 (2007); The user manual is available at http://nmag.soton.ac.uk/nmag/current/manual/html/manual.html.

[42] J. Jorzick, S. O. Demokritov, B. Hillebrands, M. Bailleul, C. Fermon, K. Y. Guslienko, A. N. Slavin, D. V. Berkov, and N. L. Gorn, Phys. Rev. Lett. **88**, 047204 (2002).

[43] K. Y. Guslienko, S. O. Demokritov, B. Hillebrands, and A. N. Slavin, Phys. Rev. B **66**, 132402 (2002).

[44] K. Y. Guslienko, R. W. Chantrell, and A. N. Slavin, Phys. Rev. B **68**, 024422 (2003).

[45] K. Y. Guslienko and A. N. Slavin, J. Magn. Magn. Mater. **323**, 2418 (2011).

[46] M. Dvornik, Y. Au, and V. V. Kruglyak, Top. Appl. Phys. **125**, 101 (2013).

[47] The spectra and mode profiles were calculated using SEMARGL http://www.magnonics.org/semargl/; M. Dvornik and V. V. Kruglyak, Phys. Rev. B **84**, 140405 (2011).

[48] R. D. McMichael and M. D. Stiles, J. Appl. Phys. **97**, 10J901 (2005).

[49] G. Gubbiotti, G. Carlotti, T. Okuno, M. Grimsditch, L. Giovannini, F. Montoncello, and F. Nizzoli, Phys. Rev. B **72**, 184419 (2005).

[50] M. Dvornik, P. V. Bondarenko, B. A. Ivanov, and V. V. Kruglyak, J Appl. Phys. **109**, 07B912 (2011).

[51] H.-J. Chia, F. Guo, L. M. Belova, and R. D. McMichael, Appl. Phys. Lett. **101**, 042408 (2012).

[52]F. Guo, L. M. Belova, and R. D. McMichael, Phys. Rev. Lett. **110**, 017601 (2013).

[53]S. V. Nedukh, S. I. Tarapov, D. P. Belozorov, A. A. Kharchenko, V. O. Golub, I. V. Kilimchuk, O. Y. Salyuk, E. V. Tartakovskaya, S. A. Bunyaev, and G. N. Kakazei, J. Appl. Phys. **113**, 17B521 (2013).

[54]L. Giovannini, F. Montoncello, F. Nizzoli, G. Gubbiotti, G. Carlotti, T. Okuno, T. Shinjo, and M. Grimsditch, Phys. Rev. B **70**, 172404 (2004).

[55]We note here analogy with systems of classical oscillators; see, e.g., L. D. Landau and E. M. Lifshitz, *Mechanics* (Butterworth-Heinemann, Oxford, 1976).

[56]S. Tacchi, F. Montoncello, M. Madami, G. Gubbiotti, G. Carlotti, L. Giovannini, R. Zivieri, F. Nizzoli, S. Jain, A. O. Adeyeye, and N. Singh, Phys. Rev. Lett. **107**, 127204 (2011).

[57]V. V. Kruglyak, P. S. Keatley, R. J. Hicken, J. R. Childress, and J. A. Katine, J. Appl. Phys. **99**, 08F306 (2006).